

Pathway-based Bayesian factor models for gene expression data

Lorenzo Mauri^{1*}, Federica Stolf^{1*}, Amy H. Herring¹, Cameron Miller², and David B. Dunson¹

*Equal contribution

¹Department of Statistical Science, Duke University, Durham, NC, USA

²Department of Medicine, Duke University School of Medicine, Durham, NC, USA

Abstract

Interpreting gene expression data requires methods that can uncover coordinated patterns corresponding to biological pathways. Traditional approaches such as principal component analysis and factor models reduce dimensionality, but latent components may have unclear biological meaning. Current approaches to incorporate pathway annotations impose restrictive assumptions, require extensive hyperparameter tuning, and do not provide principled uncertainty quantification, hindering the robustness and reproducibility of results. Here, we develop Bayesian Analysis with gene-Sets Informed Latent space (BASIL), a scalable Bayesian factor modeling framework that incorporates gene pathway annotations into latent variable analysis for RNA-sequencing data. BASIL places structured priors on factor loadings, shrinking them toward combinations of annotated gene sets, enhancing biological interpretability and stability, while simultaneously learning new unstructured components. BASIL provides accurate covariance estimates and uncertainty quantification, without resorting to computationally expensive Markov chain Monte Carlo sampling. An automatic empirical Bayes procedure eliminates the need for manual hyperparameter tuning, promoting reproducibility and usability in practice. In simulations and large-scale human transcriptomic datasets, BASIL consistently outperforms state-of-the-art approaches, accurately reconstructing gene–gene covariance, selecting the correct latent dimension, and identifying biologically coherent modules.

Main Text

High-throughput transcriptomic technologies generate measurements for tens of thousands of genes, creating data with immense promise, but also fundamental challenges in statistical analysis, especially when the number of samples is not very large. One central task in the analysis of gene expression from high-throughput RNA-sequencing data is to extract relevant biological insights. Patterns of correlated expression among genes are frequently observed in such datasets and can reflect coordinated transcriptional regulation, in which genes involved in the same pathway or cellular function are

regulated in concert to maintain synchronized activity (Myers et al., 2006). Accurate discovery of biologically relevant signals in massive dimensional noisy data is crucial for understanding the molecular mechanisms driving differences across conditions, cell types, or perturbations. Matrix factorization techniques, such as principal component analysis (PCA) or factor analysis, are widely used to infer components of variation in multivariate gene expression data. These methods rely on low-dimensional latent variable representations that can offer biologically meaningful interpretations. Factor models can be used to infer gene co-expression networks by identifying pairs of genes whose expression profiles are significantly associated across samples (Sekula et al., 2020). Constructing such networks is a key objective in many biological studies, as it enables researchers to uncover novel gene interactions and functional relationships.

Structured matrix factorizations have been proposed to incorporate biological knowledge. Examples include leveraging gene–gene interaction networks to guide factors towards known pathways (Elyanow et al., 2020) and using gene perturbation data to associate factors with perturbation effects in single-cell CRISPR screens (Zhou et al., 2023). Other contributions target scRNA-seq data (Buettner et al., 2017; Kunes et al., 2024). In this work, we focus on bulk RNA-sequencing data and use gene sets as prior information. The state of the art in this setting is PLIER (pathway-level information extractor) (Mao et al., 2019), a matrix factorization approach that maps gene expression data into a low-dimensional space. Integrating pathway-informed annotations improves interpretability by yielding latent components aligned with known pathways. The PLIER framework has been extensively refined (Pividori et al., 2023; Taroni et al., 2019; Zhang et al., 2024), but key problems remain. First, it restricts factor loadings to be positive, which rules out commonly observed and biologically meaningful negative correlations (Zeng and Li, 2010; Tu et al., 2015). Hence, PLIER estimates need ad hoc post-processing, which results in sub-optimal accuracy, as we will show in our numerical experiments. PLIER is highly sensitive to hyperparameter choices, requiring computationally expensive tuning and potentially leading to poor recovery of the empirical gene correlation structure (fig. 1b). Furthermore, PLIER and related methods (e.g. Buettner et al. (2017)) do not provide uncertainty quantification (UQ) in the inferred gene–gene covariance.

To overcome these limitations, we develop Bayesian Analysis with gene-Sets Informed Latent space (BASIL). BASIL is based on a probabilistic matrix factorization framework and specifically adopts a Bayesian learning paradigm, which has several advantages in this setting. Bayesian methods offer a natural way to incorporate known gene sets through structured prior distributions and provide straightforward uncertainty quantification. The proposed approach projects high-dimensional gene expression data onto a low-dimensional set of latent factors, each representing an interpretable combination of gene sets. By integrating knowledge of gene sets, these latent variables capture structured variation in expression and provide meaningful insights into molecular processes. BASIL

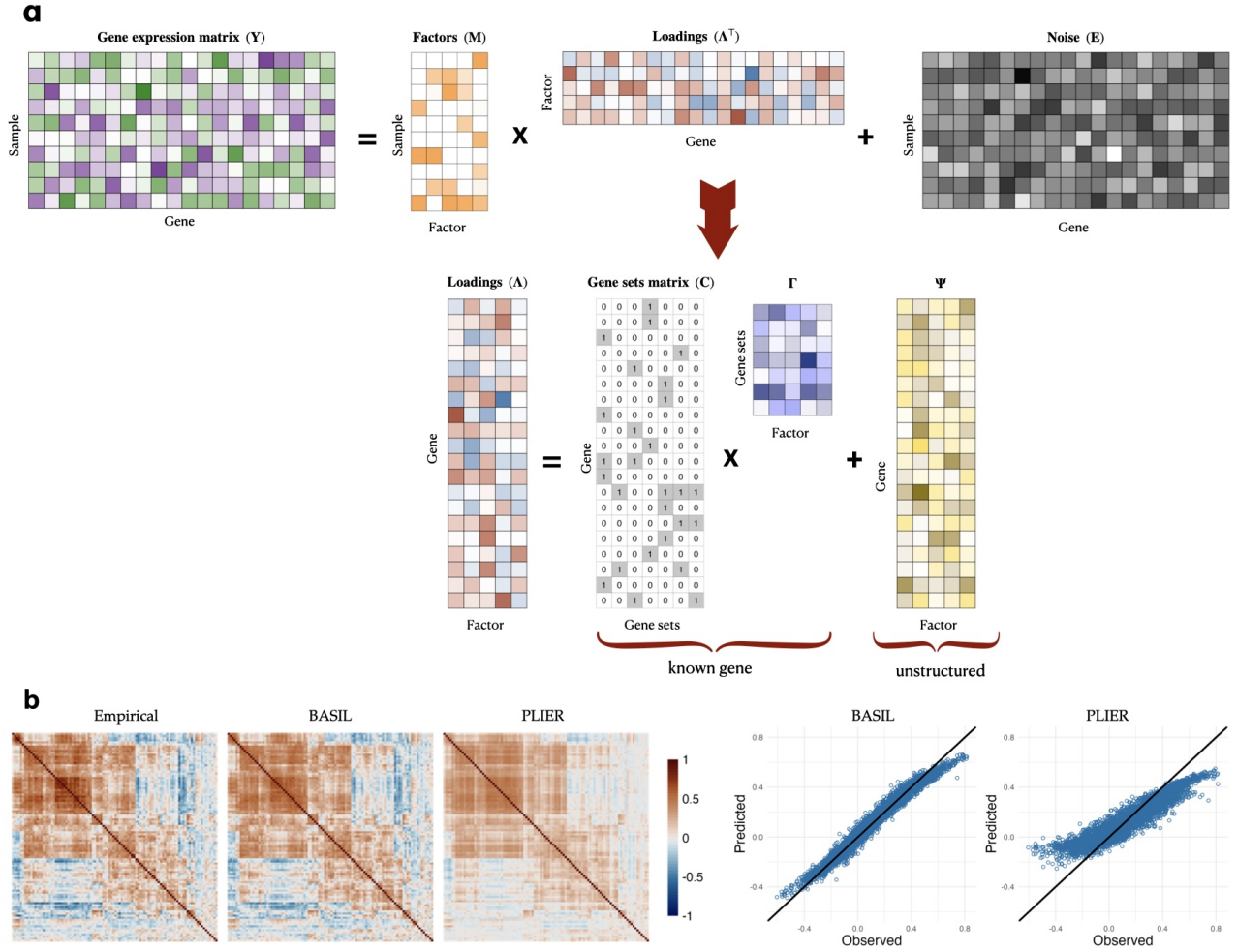


Figure 1: **BASIL overview.** **a**, BASIL is a two-layer matrix factorization approach: in the top layer the gene expression matrix (Y) is factorized as the product of a small number of latent variables (M) and their corresponding gene weights (Λ); in the hierarchical layer BASIL exploits prior gene ontology – the binary gene set membership matrix C – in the definition of Λ . **b**, Empirical gene-gene correlation matrix computed from a subset of 100 genes for a gene expression dataset (global fever data) and correlation matrices estimated with BASIL and PLIER, reconstructed through latent variable factorization. The scatter plots show observed versus predicted correlation values.

relies on a scalable and computationally efficient algorithm that enables fast inference even when analyzing 10,000s of genes. We assess performance through extensive simulation studies and analysis of gene expression datasets. The results demonstrate that BASIL not only identifies biologically significant gene modules but also achieves superior predictive accuracy compared to state of the art approaches.

Results

Overview of gene sets informed factor models

BASIL is a Bayesian factor model that incorporates biological pathway information through a structured prior distribution. The input of BASIL consists of two matrices: a normalized gene expression matrix across samples (Y) and a binary gene membership matrix (C) based on prior knowledge. The matrix Y may consist of gene expression data from RNA sequencing or microarray experiments in which rows represent samples and columns represent genes. Each column of C corresponds to a molecular pathway, gene ontology set or any other predefined gene collection of interest. The proposed approach factorizes the gene expression matrix into the product of the factor matrix (M) and the gene weight matrix (Λ) plus a residual noise matrix (E).

To incorporate gene pathway information, BASIL defines a hierarchical structure in the gene weights matrix, introducing a second layer in the model (fig. 1a). Specifically, we assume that Λ is the sum of two components: the product of the gene set matrix (C) and a linkage matrix Γ , and a newly discovered gene set matrix (Ψ). The matrix Γ is a graphical matrix that encodes the association between latent variables and gene sets or pathways, promoting a biologically meaningful interpretation of the latent space. This structure allows for the incorporation of known gene ontology information while addressing the fact that many genes are not in any existing gene set. By modeling these two components separately, BASIL enhances both interpretability and flexibility. This represents a key advantage over PLIER (Mao et al., 2019), which does not explicitly distinguish between structured and unstructured sources of variability.

The unknown quantities that we want to infer from the data are the factor matrix M , the gene weight matrix Λ (defined through Ψ and Γ) and the variance of the residual noise matrix E . In a Bayesian framework, we specify a suitable prior for each unknown. We assume a standard normal prior distribution for the elements of M and an inverse gamma prior for the variance of the residual noise matrix E . Using the definition of Λ , which separates the two sources of variability, we use normal shrinkage priors centered on zero for the elements of these two components of Λ . Shrinkage priors reduce the mean square error and enable estimation in cases in which the number of genes exceeds the number of samples. We allow for two different levels of shrinkage, by specifying different variance parameters controlling the magnitude of Ψ and Γ (see Methods). This structure avoids strong assumptions about the underlying biological processes while enabling BASIL to adaptively infer gene-pathway relationships from the data.

Bayesian methods generally rely on Markov chain Monte Carlo (MCMC) sampling or variational inference for posterior computation. MCMC algorithms are computationally expensive, while variational approximations often massively underestimate uncertainty, hindering the reliability of interval estimates.

Here, we develop a fast and accurate algorithm that exploits a blessing of dimensionality to motivate pre-estimation of the latent factors (Chattopadhyay et al., 2024; Mauri and Dunson, 2025a). The inferential procedure is fast and avoids MCMC while producing intervals with correctly calibrated coverage. Hence, BASIL produces valid confidence intervals. To enhance interpretability, BASIL applies factor rotations to induce sparsity, activating only a subset of gene factors per subject, which can then be interpreted via their loadings and associations with known gene sets. In addition to producing much more accurate results, BASIL offers two major advantages over PLIER. First, BASIL provides uncertainty quantification, allowing an assessment of the variability around factor estimates. Second, BASIL avoids the need for intensive hyperparameter tuning, making the inference process more efficient, stable, and user-friendly. The number of latent factors is automatically selected by minimizing an information criterion, which consistently identified the correct number in our simulation studies. Additionally, the shrinkage prior coefficients are determined by an empirical Bayes approach (Morris, 1983) avoiding manual tuning.

Simulation study shows the effectiveness of BASIL

We evaluated the performance of BASIL compared to state of the art methods across several metrics: estimation accuracy, computational efficiency, uncertainty quantification, and parameter interpretability. We simulated gene expression data in two different scenarios. The first, referred to as ‘high ontology signal’, reflects a setting in which the variability in the gene weights matrix Λ is primarily driven by gene ontology information, with low unstructured variability. The second scenario, referred to as ‘low ontology signal’, is dominated by unstructured variability, accounting for the fact that biological signal in many genes is not fully characterized by known gene sets. The former represents an ideal case where known gene sets strongly inform latent gene associations, while the latter captures realistic settings where gene ontology information may be incomplete or inaccurate. In practice, this is implemented by assigning different values to the variance parameters associated with the structured (Γ) and unstructured (Ψ) components of the gene weight matrix. In both settings, we considered two different values for the number of genes - 1,000 and 3,000 - 10 latent factors and 500 samples. For each configuration, we reproduce the experiments 25 times. We obtain the matrix of gene sets C using the `msigdbr` R package that provides access to gene sets from the Molecular Signatures Database.

To evaluate the performance of BASIL in estimation accuracy, we compute the error in reconstructing the true gene co-expression matrix. For comparison, we also ran PLIER (Mao et al., 2019) and ROTATE (Ročková and George, 2016), a widely used factor model based on a computationally efficient algorithm that does not allow prior information on gene sets. BASIL outperforms competitors in all scenarios (fig. 2a) in recovering the true gene co-expression matrix, showing attractive results in latent factor inference. In addition to being very accurate, BASIL is also fast to run, especially compared to PLIER

(fig. 2b). Indeed, BASIL runs in a few seconds on the simulated datasets and is approximately 30 times faster than PLIER on average for our experiments.

A critical issue in low-rank matrix factorization is the choice of the latent dimension, i.e. the number of factors. In our experiments, BASIL consistently recovered the true number of factors in all scenarios, while PLIER significantly overestimated it (fig. 2c). This tendency toward overestimation not only introduces bias in factor estimation but also results in less parsimonious models, making the biological interpretation of the factors more challenging.

To assess BASIL’s performance in uncertainty quantification, we evaluated the frequentist coverage of the posterior credible intervals for the gene covariance matrix (fig. 2d). Specifically, we evaluated over many repeated datasets generated under the same conditions the proportion of cases in which the posterior credible intervals of BASIL contained the true covariance values. A well-calibrated method should yield coverage frequencies close to the nominal level used to construct the intervals. This approach provides a standard metric for determining whether the uncertainty estimated by a Bayesian method is accurate and practically reliable. We recall that both PLIER and ROTATE produce only point estimates of the gene covariance matrix, without offering any means to quantify uncertainty. For this reason, we exclude them from the uncertainty quantification experiments. Across all scenarios, the average coverage of the entrywise intervals is close to the nominal value 0.95, providing support for BASIL in terms of producing well-calibrated credible intervals.

We highlight two key parameters in BASIL, the prior variances for the two components of Λ modeling the signal explained by the known and unknown pathways, which we denote as τ_Ψ^2 and τ_Γ^2 , respectively. The ratio between τ_Γ^2 and τ_Ψ^2 serves as an indicator of how informative gene ontology knowledge is in the latent factor model. A ratio of less than one indicates substantial unstructured variability, while a ratio above one implies that the majority of the signal in the data aligns to known gene ontologies. Estimates of this ratio grow as the ontology signal increases (fig. 2e). BASIL’s adaptivity to the true ontology signal is illustrated by focusing on two extreme scenarios: i) all variability is explained by known pathways ($\Psi = 0$); ii) all variability is explained by novel pathways ($\Gamma = 0$). We show that under regularity conditions (Methods) when $\Psi = 0$, the contribution of new pathways is automatically reduced to zero and BASIL simplifies to a model that only uses known pathways, while, if $\Gamma = 0$, the contribution from known pathways vanishes.

Application to whole-blood RNA-seq data

We apply BASIL to the validation dataset provided in [Mao et al. \(2019\)](#), which comprises human whole-blood samples assayed by RNA sequencing. The dataset consists of 36 samples for 5892 genes. We constructed the pathway matrix C using 606 pathways that included 61 cell-type markers and 555 canonical pathways from the Molecular Signatures Database. The criterion in (5) selects $k = 8$ factors

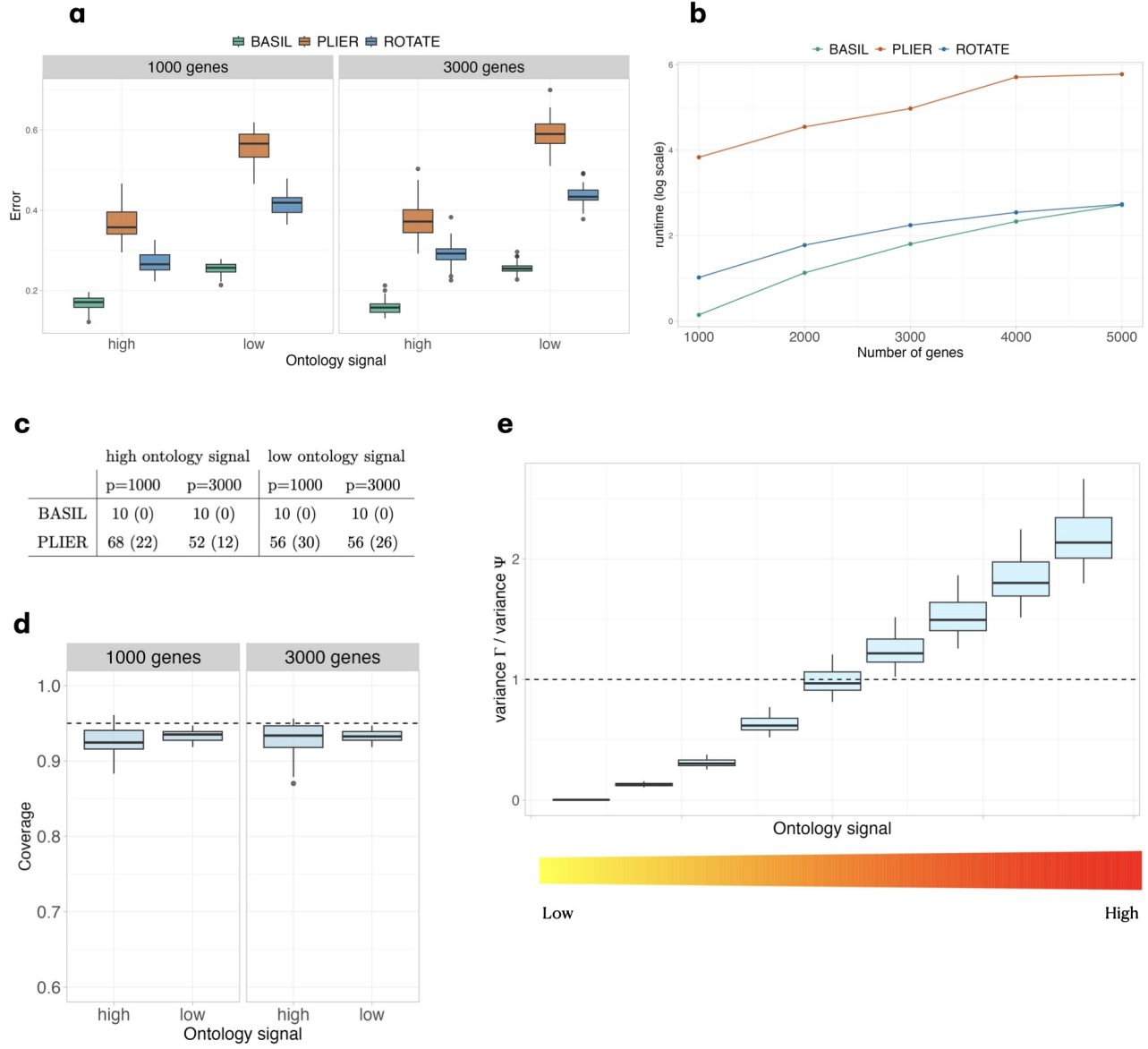


Figure 2: Simulated data results. **a**, Performance of BASIL, ROTATE and PLIER in estimation accuracy for the gene co-expression matrix in low and high ontology signal scenarios over the 25 replications. **b**, Mean runtime over 25 replications of BASIL, ROTATE and PLIER with datasets simulated under different values for the number of genes in the ‘high ontology signal’ scenario. The results are in seconds on a logarithmic scale. **c**, BASIL and PLIER estimations of the number of latent factors across the two scenarios. We report median and interquartile range over 25 replications. **d**, Frequentist coverage of 95% credible intervals for the gene covariance matrix by BASIL over the 25 replications across the two scenarios. **e**, Ratio between the estimated variances for Γ and Ψ as the ontology signal increases. The plot shows the results over 25 replications for each setting.

and the estimates of the shrinkage parameters τ_{Γ}^2 and τ_{Ψ}^2 are 0.82 and 0.29, respectively, suggesting that pathway information plays an important role and should be considered in the model.

The high dimensionality of the dataset combined with the low sample size induces non-negligible uncertainty in the inferred gene-gene covariance matrix. Methods like PLIER neglect such uncertainty, while BASIL offers a way to seamlessly focus on relevant associations, and exclude spurious ones, via the posterior distribution of quantities of interest. For example, Figure 3a shows the empirical gene-gene correlation matrix for the subset of the 100 genes with the largest empirical variance and the estimates of BASIL and PLIER. In the third panel, we display the BASIL posterior mean of the correlation matrix, after zeroing out the entries for which the corresponding 95% credible interval included zero. Roughly 85% of the possible pairs of genes did not display a statistically significant correlation value. This dramatically decreases the number of associations to be considered, facilitating downstream analysis and interpretability.

We show the resulting gene network in Fig. 3b. BASIL identifies two large clusters that contain genes associated with neutrophil granules and activation. The first includes genes such as arginase-1 (ARG1), matrix metalloproteinase-9 (MMP9), and peptidoglycan recognition protein 1 (PGLYRP1), which are known markers of neutrophil function (Yang et al., 2020). The second group includes neutrophil elastase (ELANE), myeloperoxidase (MPO), azurocidin (AZU1) and defensin α 4 (DEFA4), reflecting the co-expression of azurophilic granule proteins in neutrophils (Calzetti et al., 2022). These genes have previously been identified as a coordinated module under different conditions (Hemmat et al., 2020). There is also a third cluster with genes specific to erythrocytes and erythropoiesis, such as erythroid 5'-aminolevulinate synthase (ALAS2), glycophorin B (GYPB) and erythrocyte membrane anion exchanger (SLC4A1). These genes are well known to be co-expressed in leukocyte-derived data reflecting erythropoietic adaptation (Trudel et al., 2024). While BASIL yields a sparse network with three well-separated, biologically interpretable clusters, PLIER's network is considerably denser, with numerous weak or spurious correlations obscuring the underlying modular structure. This demonstrates BASIL's superior ability to separate signal from noise, resulting in a sparse network that enhances biological interpretability and facilitates the identification of functionally relevant gene modules.

We refer to the Methods section for experiments that compare the out-of-sample predictive accuracy of competing methods, where BASIL displays state-of-the-art performance.

Application to global fever data

We next applied BASIL to transcriptomic data from patients with confirmed viral or bacterial infections of varying etiologies, as well as from individuals with non-infectious disease mimics (Ko et al., 2023). The study included 294 patients recruited in the United States (152) and Sri Lanka (142) and ensured a balanced representation across demographic and clinical subgroups. RNA was extracted from whole-

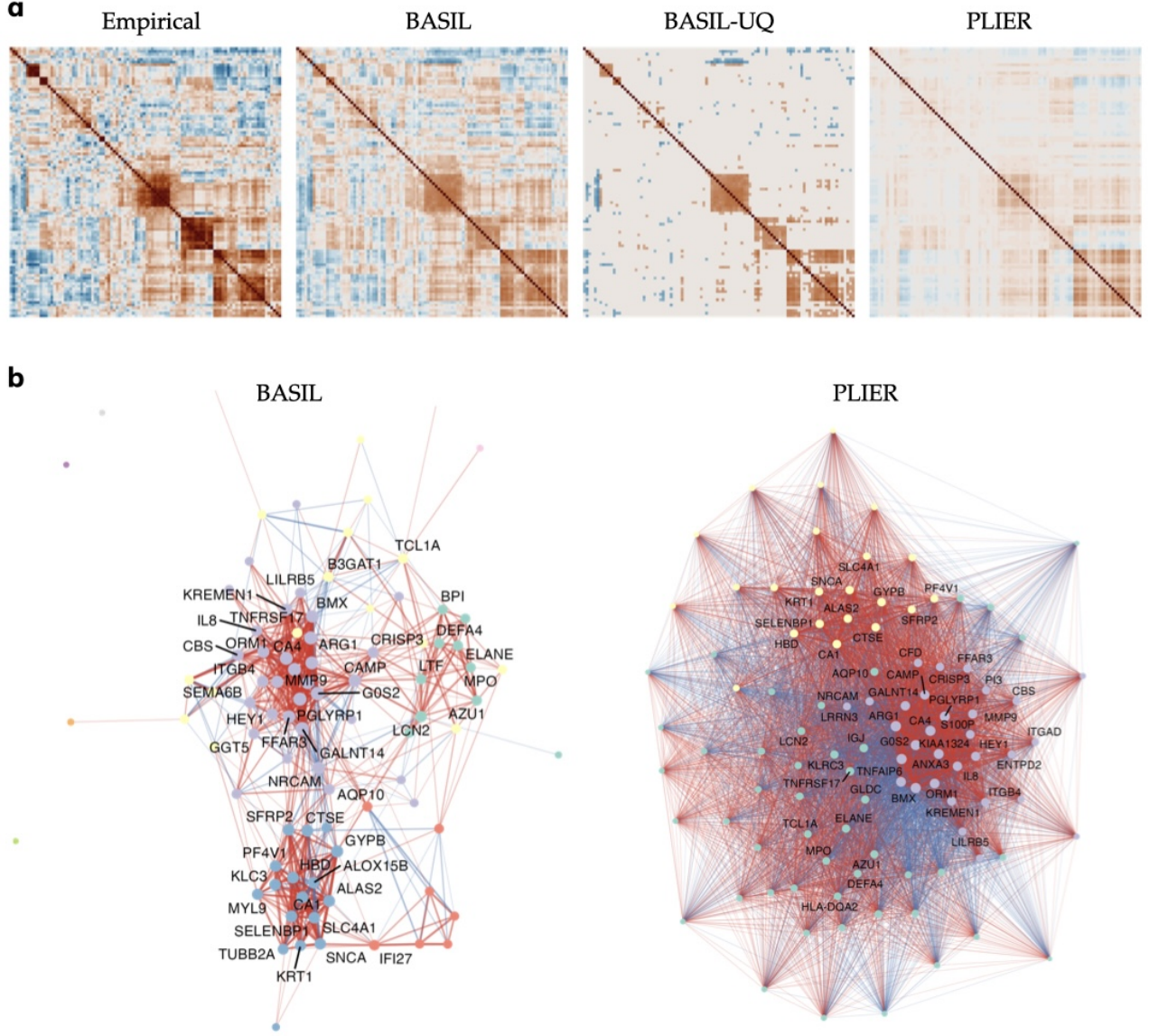


Figure 3: Whole-blood RNA-seq data correlation analysis. **a**, Empirical gene-gene correlation matrix for a subset of 100 genes and correlation matrices estimated with BASIL and PLIER. The two middle panels show the BASIL posterior mean of the correlation matrix without and with zeroing out the entries for which the corresponding 95% credible interval included 0. **b**, Gene network plot for BASIL including only statistically significant correlations and PLIER. Positive (negative) correlations are shown in red (blue).

blood samples and sequenced to measure gene expression in two batches, with batch effects corrected for by using overlapping samples. The authors filtered out low expression genes and normalized the data and the resulting dataset included 14,386 genes. Details on data assembly, along with the full list of pathogens, are provided in the supplementary materials. We constructed the pathway matrix C

using gene sets from the Gene Ontology Molecular Function collection in the Molecular Signatures Database. The criterion introduced in the Methods section selects 19 factors and the ratio between τ_{Γ}^2 and τ_{Ψ}^2 is 8.2, suggesting that gene ontology contributes substantially in modeling the gene covariance. Fig. 1b compares gene-gene correlation matrices estimated by BASIL and PLIER with the empirical correlation matrix. BASIL's estimates are more accurate, particularly for the negative coefficients, providing more robust and reliable results.

The structure introduced by BASIL on the gene weight matrix enables direct interpretation in terms of gene ontology. Specifically, the graphical matrix Γ links latent factors to biological pathways, allowing functional explanation of factors using established gene ontology terms. To focus on statistically significant associations, we applied the BASIL uncertainty quantification procedure (Methods) and set all entries in Γ to zero whose 95% credible intervals included zero (about 40% of the matrix entries). Our analysis concentrates on the first ten factors, representing the components that explain the largest proportion of variability in the data. The results are shown in Fig. 4a, displaying for each factor the five pathways with the largest absolute coefficients.

The inferred factors define interpretable axes of molecular function that delineate signaling, transport, and immune regulatory pathways. The most prominent signal is phosphoinositide phosphatase activity: three factors (Factors 1, 2 and 7) are dominated by gene ontology terms for dephosphorylation of phosphatidylinositol derivatives, indicating that variation in phosphoinositide turnover is a major driver of expression heterogeneity. Beyond these core signaling modules, several factors capture structured trade-offs between functional programs. Factor 4 showed an innate-immune signature, linking high ATPase-coupled ion transport with low Toll-like receptor 4 (TLR4) binding activity, which mediates recognition of lipopolysaccharide (LPS) and triggers inflammatory responses (Luo et al., 2025; Park and Lee, 2013). This immune-versus-transport contrast likely reflects heterogeneity between inflammatory and non-immune blood cell populations, highlighting the value of allowing both positive and negative loadings to capture meaningful biological oppositions. Similarly, Factors 2 and 9 revealed bidirectional patterns that would be obscured in approaches that constrain all loadings to be positive, such as PLIER.

Fig. 4b shows what fractions of systematic variability are explained by known pathways ($C\Gamma$) or unknown components (Ψ) for the 50 genes with the highest variability. The variability of the gene C-X-C motif chemokine 10 (NM-001565 in the figure) is entirely explained by known pathways. This gene encodes a potent pro-inflammatory chemokine induced by IFN- γ and is part of a well-characterized immune pathway. For instance, CXCL10 is included in the KEGG Chemokine Signaling pathway and the Hallmark Inflammatory Response gene set (Liu et al., 2011; Ko et al., 2023). Hence, when interferon or inflammation pathways are active, CXCL10 is coordinately upregulated. Similarly, we note several IFI27 transcripts with more than half of their variation explained by known pathways. IFI27

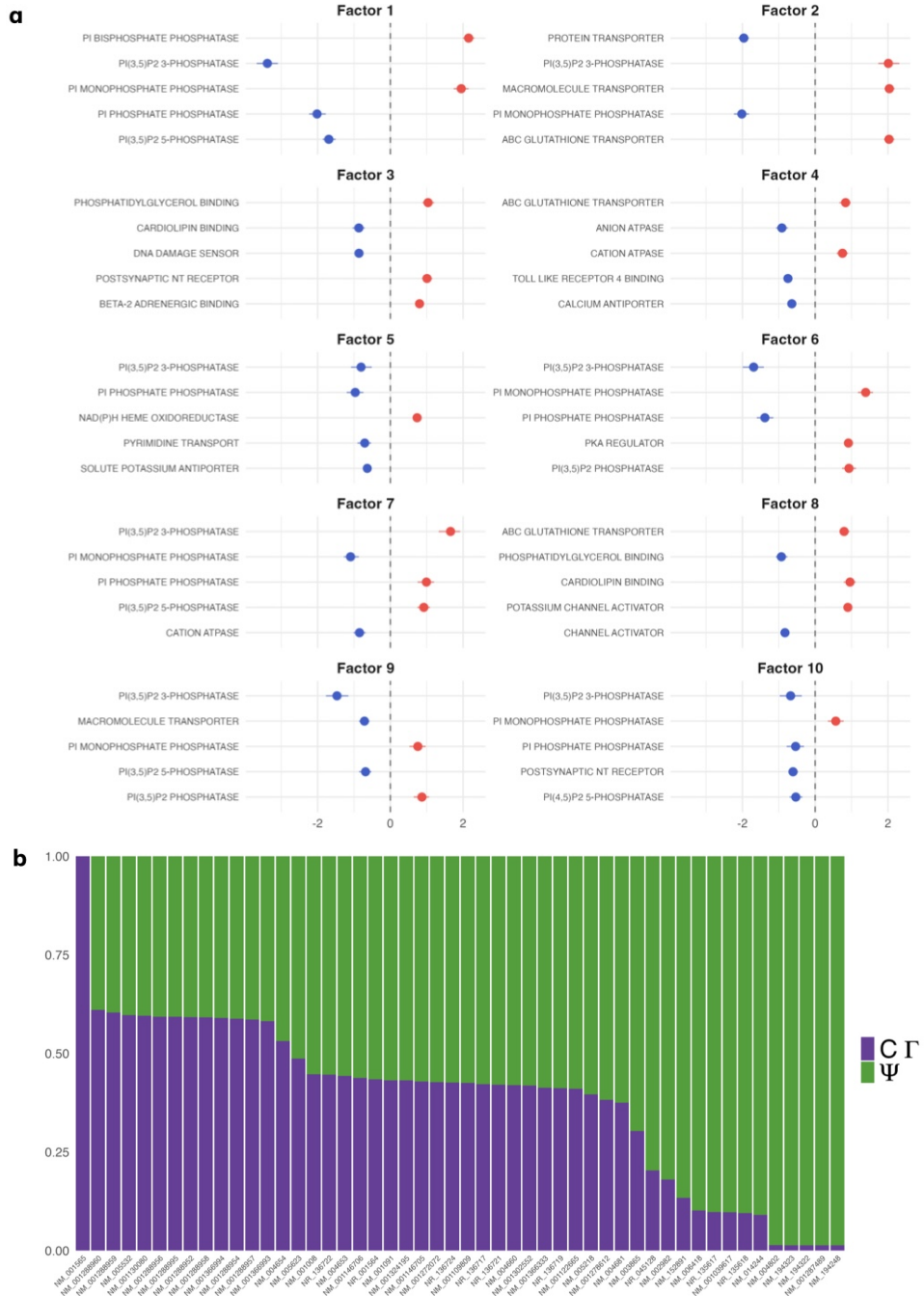


Figure 4: **Global fever data known pathway and unstructured components.** **a**, Top 5 pathways for the first ten factors of Γ after zeroing out the entries for which the corresponding 95% credible intervals included 0. The plot shows the posterior mean and 95% posterior credible interval for each element. Positive (negative) values are shown in red (blue). **b**, Proportions of variance explained by known (Γ) versus unknown (Ψ) pathways for a subset of 50 genes.

is upregulated by IFN- α/β during antiviral responses (Shojaei and McLean, 2025). The dominance of CXCL10 and IFI27 indicates that type I/II interferon-driven inflammation is a major source of structured expression variance in the dataset. These genes are markers of an active immune response to infection or inflammatory challenge. Therefore, the top genes confirm that canonical immune pathways (especially interferon signaling) are a predominant, explainable source of gene expression variation in this dataset. Among the genes with the lowest fraction of variability explained by known pathways, we note some Otoferlin (OTOF) transcripts. OTOF acts as a calcium sensor for synaptic vesicle fusion in auditory inner hair cells (Michalski et al., 2017) but is not expressed in immune or inflammatory cells.

The BASIL factors were interpreted by applying gene set enrichment analysis (GSEA) to the loadings separately for each factor. While the Gene Ontology Molecular Function collection was used to construct the factors to reduce selection bias in gene set curation, generating contextualized interpretations using this collection is challenging. Therefore, the human Reactome pathways (Ligtenberg, 2025) were used in the GSEA. We report the detailed GSEA workflow in the supplementary material, including the procedures used to generate the pathway network diagrams shown in Figure 5a.

Figure 5b displays the factor annotations for the first ten factors resulting from the GSEA. In summary, the factor analysis identifies biologically interpretable axes of host immune variation, several of which align with established immune paradigms. In the supplementary material, we report the pairwise plots for the elements of the first ten factors, colored by different pathogens. For example, Factor 2 is enriched for an HIV infection gene set and ribosomal/translation pathways, suggesting a host state prioritizing protein synthesis—consistent with responses to viral pathogens such as influenza or dengue that depend on host ribosomes for replication (Walsh and Mohr, 2011). Notably, some intracellular bacteria elicit similar interferon-dominated responses. Coxiella and Rickettsia infections, for instance, activate interferon-stimulated genes (Colonne et al., 2011), reflecting their intracellular lifestyle and reliance on host cellular machinery. Factor 10 is enriched for broad immune and stress-response pathways and uniquely shows positive enrichment for inflammatory signaling. The involvement of IL-1 and NF- κ B pathways is characteristic of bacterial infections, as pathogens such as Staphylococcus and Streptococcus strongly activate NF- κ B and inflammasome signaling (Liu et al., 2017). Other factors capture variation in immune cell metabolic and proliferative states (Factors 3, 4, 8, and 9) or systemic stress responses (Factor 7).

Discussion

We have presented BASIL, a Bayesian matrix factorization framework for analyzing bulk RNA-sequencing data that integrates gene set annotations to extract biologically interpretable latent factors. Through comprehensive simulation studies and real data applications, we demonstrated that BASIL offers substantial improvements over existing methods in several critical aspects: accurate recovery

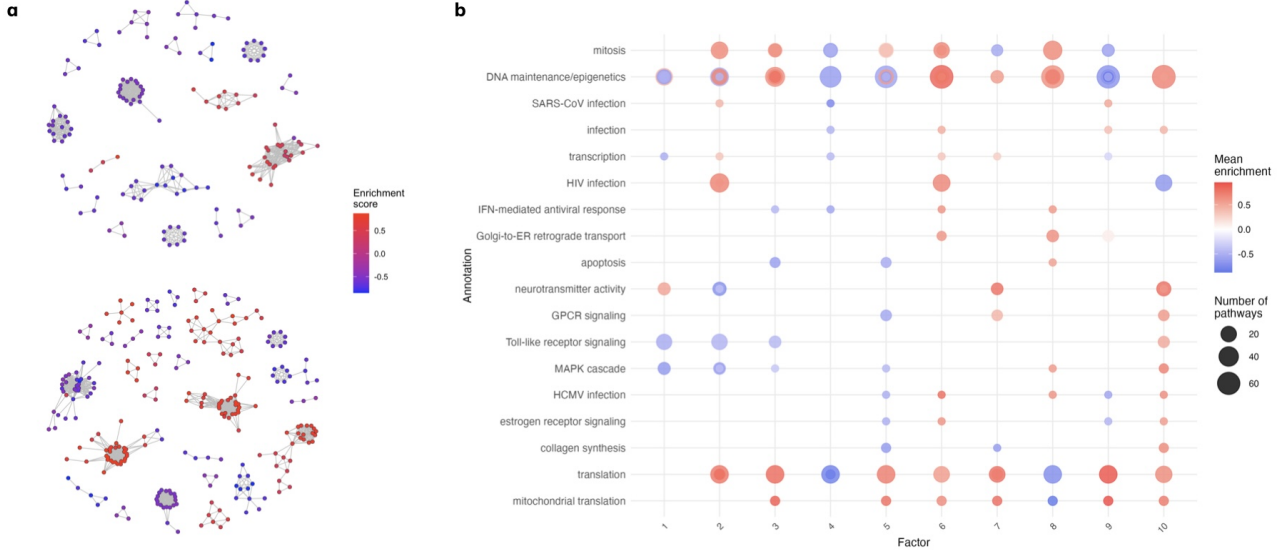


Figure 5: **Enrichment analysis for global fever data.** **a**, Network maps for the first two factors, following filtering and community detection, overlaid with the enrichment scores. **b**, Factor annotations for the first ten factors.

of gene co-expression structure, rigorous uncertainty quantification, and enhanced interpretability of latent components. A key advantage of BASIL is its fully probabilistic framework, which avoids the ad hoc post-processing required by methods like PLIER and naturally provides uncertainty quantification without the instability and computational expense of cross-validation approaches. BASIL is computationally efficient, making it broadly applicable without extensive tuning or computational resources.

While our proposed framework addresses several limitations in the current literature, there remain many directions for further development. First, while we focused on bulk RNA-seq data, the framework could be extended to single-cell RNA-sequencing, where additional structure (e.g., cell type annotations, temporal dynamics) could be incorporated. Other interesting directions include multi-study or multi-view settings, that are specifically designed for integrating diverse data modalities such as multi-omics. One promising direction would be extending scalable approaches in those settings (Mauri et al., 2025; Mauri and Dunson, 2025b) to incorporate gene ontologies. Finally, it would be interesting to extend our methodology to model clustered data, letting the factor loadings to vary across clusters. This would allow the grouping of patients into biologically interpretable clusters based on their RNA-sequencing data, with potential applications to precision medicine and individualized treatment development.

Acknowledgments

This work was partially supported by the National Institute of Health (NIH) (grants R01-ES035625, R01-ES027498, P42-ES010356, R01-AI155733), the Office of Naval Research (ONR) (grant N000142412626), the European Research Council under the European Union’s Horizon 2020 research and innovation (grant agreement No 856506), and the National Science Foundation (NSF) (IIS-2426762).

Author contributions

Lorenzo Mauri (LM) and Federica Stolf (FS) worked on developing the specific details of the BASIL method, implementing the approach, and drafting the manuscript. Cameron Miller provided genomic expertise in interpreting the results. Amy Herring suggested the initial directions in terms of evaluating and improving on PLIER while also providing guidance, and David Dunson proposed a rough version of the initial BASIL approach, co-supervised LM and FS’s work, and helped revise the draft.

Data availability

Both RNA-seq datasets used in this study are publicly available. The validation dataset provided in [Mao et al. \(2019\)](#) is available in the PLIER R package, and the global fever dataset was downloaded from the GEO (accession nos. GSE211567).

Code availability

The R package implementing BASIL is available at <https://github.com/federicastolf/BASIL>. The code to reproduce the analyses, figures, and results in this paper is available at https://github.com/federicastolf/BASIL_paper.

References

Bai, J. (2003). Inferential theory for factor models of large dimensions. *Econometrica* 71(1), 135–171.

Buettner, F., N. Pratanwanich, D. J. McCarthy, J. C. Marioni, and O. Stegle (2017). f-scLVM: Scalable and versatile factor analysis for single-cell rna-seq. *Genome Biology* 18(1), 212.

Calzetti, F., G. Finotti, N. Tamassia, F. Bianchetto, M. Castellucci, S. Canè, S. Lonardi, C. Cavallini, A. Matte, S. Gasperini, I. Signoretto, F. Benedetti, M. Bonifacio, W. Vermi, S. Ugel, V. Bronte, C. Tecchio, P. Scapini, and M. Cassatella (2022, 04). CD66b-CD64-CD115 cells in the human bone marrow represent neutrophil-committed progenitors. *Nature Immunology* 23, 679–691.

Chattopadhyay, S., A. R. Zhang, and D. B. Dunson (2024). Blessing of dimension in Bayesian inference on covariance matrices. *arXiv preprint arXiv:2404.03805*.

Chen, Y. and X. Li (2021). Determining the number of factors in high-dimensional generalized latent factor models. *Biometrika* 109(3), 769–782.

Chen, Y., X. Li, and S. Zhang (2019). Joint maximum likelihood estimation for high-dimensional exploratory item factor analysis. *Psychometrika* 84(1), 124–146.

Chen, Y., X. Li, and S. Zhang (2020). Structured latent factor analysis for large-scale data: Identifiability, estimability, and their implications. *Journal of the American Statistical Association* 115(532), 1756–1770.

Colonne, P. M., A. Sahni, and S. K. Sahni (2011). Rickettsia conorii infection stimulates the expression of isg15 and isg15 protease ubp43 in human microvascular endothelial cells. *Biochemical and Biophysical Research Communications* 416(1-2), 153–158.

Csárdi, G., T. Nepusz, V. Traag, S. Horvát, F. Zanini, D. Noom, K. Müller, D. Schoch, and M. Salmon (2026). *igraph: Network Analysis and Visualization in R*. R package version 2.2.1.

Elyanow, R., B. Dumitrescu, B. E. Engelhardt, and B. J. Raphael (2020). netNMF-sc: Leveraging gene–gene interactions for imputation and dimensionality reduction in single-cell expression analysis. *Genome Research* 30(2), 195–204.

Hemmat, N., A. Derakhshani, H. Bannazadeh Baghi, N. Silvestris, B. Baradaran, and S. De Summa (2020). Neutrophils, crucial, or harmful immune cells involved in coronavirus infection: A bioinformatics study. *Frontiers in Genetics* 11, 641.

Kaiser, H. F. (1958). The varimax criterion for analytic rotation in factor analysis. *Psychometrika* 23(3), 187–200.

Ko, E. R., M. E. Reller, L. G. Tillekeratne, C. K. Bodinayake, C. Miller, T. W. Burke, R. Henao, M. T. McClain, S. Suchindran, B. Nicholson, et al. (2023). Host-response transcriptional biomarkers accurately discriminate bacterial and viral infections of global relevance. *Scientific Reports* 13(1), 22554.

Korotkevich, G., V. Sukhov, N. Budin, B. Shpak, M. N. Artyomov, and A. Sergushichev (2016). Fast gene set enrichment analysis. *biorxiv*, 060012.

Kunes, R. Z., T. Walle, M. Land, T. Nawy, and D. Pe'er (2024). Supervised discovery of interpretable gene programs from single-cell data. *Nature Biotechnology* 42(7), 1084–1095.

Lee, S. M., Y. Chen, and T. Sit (2024). A latent variable approach to learning high-dimensional multivariate longitudinal data. *arXiv preprint arXiv:2405.15053*.

Ligtenberg, W. (2025). *reactome.db: A set of annotation maps for reactome*. R package version 1.92.0.

Liu, M., S. Guo, J. M. Hibbert, V. Jain, N. Singh, N. O. Wilson, and J. K. Stiles (2011). Cxcl10/ip-10 in infectious diseases pathogenesis and potential therapeutic implications. *Cytokine & Growth Factor Reviews* 22(3), 121–130.

Liu, T., L. Zhang, D. Joo, and S.-C. Sun (2017). Nf- κ b signaling in inflammation. *Signal transduction and targeted therapy* 2(1), 1–9.

Luo, R., Y. Yao, Z. Chen, and X. Sun (2025). An examination of the LPS-TLR4 immune response through the analysis of molecular structures and protein–protein interactions. *Cell Communication and Signaling* 23(1), 142.

Mao, W., E. Zaslavsky, B. M. Hartmann, S. C. Sealfon, and M. Chikina (2019). Pathway-level information extractor (PLIER) for gene expression data. *Nature Methods* 16(7), 607–610.

Mauri, L., N. Anceschi, and D. B. Dunson (2025). Spectral decomposition-assisted multi-study factor analysis. *arXiv preprint arXiv:2502.14600*.

Mauri, L. and D. B. Dunson (2025a). Factor pre-training in Bayesian multivariate logistic models. *Biometrika*, asaf056.

Mauri, L. and D. B. Dunson (2025b). Inference on covariance structure in high-dimensional multi-view data. *arXiv preprint arXiv:2509.02772*.

Michalski, N., J. D. Goutman, S. M. Auclair, J. Boutet de Monvel, M. Tertrais, A. Emptoz, A. Parrin, S. Nouaille, M. Guillon, M. Sachse, D. Ceric, A. Bahloul, J.-P. Hardelin, R. B. Sutton, P. Avan, S. S. Krishnakumar, J. E. Rothman, D. Dulon, S. Safieddine, and C. Petit (2017). Otoferlin acts as a Ca^{2+} sensor for vesicle fusion and vesicle pool replenishment at auditory hair cell ribbon synapses. *eLife* 6, e31013.

Morris, C. N. (1983). Parametric empirical Bayes inference: Theory and applications. *Journal of the American statistical Association* 78(381), 47–55.

Myers, C. L., D. R. Barrett, M. A. Hibbs, C. Huttenhower, and O. G. Troyanskaya (2006). Finding function: evaluation methods for functional genomic data. *BMC Genomics* 7, 1–15.

Pagès, H., M. Carlson, S. Falcon, and N. Li (2025). *AnnotationDbi: Manipulation of SQLite-based annotations in Bioconductor*. R package version 1.70.0.

Park, B. S. and J.-O. Lee (2013). Recognition of lipopolysaccharide pattern by TLR4 complexes. *Experimental & Molecular Medicine* 45(12), e66–e66.

Pividori, M., S. Lu, B. Li, C. Su, M. E. Johnson, W.-Q. Wei, Q. Feng, B. Namjou, K. Kiryluk, I. J. Kullo, et al. (2023). Projecting genetic associations through gene expression patterns highlights disease etiology and drug mechanisms. *Nature Communications* 14(1), 5562.

Ročková, V. and E. I. George (2016). Fast Bayesian factor analysis via automatic rotations to sparsity. *Journal of the American Statistical Association* 111(516), 1608–1622.

Sekula, M., J. Gaskins, and S. Datta (2020). A sparse Bayesian factor model for the construction of gene co-expression networks from single-cell rna sequencing count data. *BMC Bioinformatics* 21(1), 361.

Shojaei, M. and A. S. McLean (2025). Interferon-stimulated gene IFI27 as a multifaceted candidate target in precision medicine. *Trends in Immunology* 46(3), 219–228.

Taroni, J. N., P. C. Grayson, Q. Hu, S. Eddy, M. Kretzler, P. A. Merkel, and C. S. Greene (2019). MultiPLIER: A transfer learning framework for transcriptomics reveals systemic features of rare disease. *Cell Systems* 8(5), 380–394.

Trudel, G., D. Stratis, L. Rocheleau, et al. (2024). Transcriptomic evidence of erythropoietic adaptation from the international space station and from an earth-based space analog. *npj Microgravity* 10(55).

Tu, X., Y. Wang, M. Zhang, and J. Wu (2015). Using formal concept analysis to identify negative correlations in gene expression data. *IEEE/ACM Transactions on Computational Biology and Bioinformatics* 13(2), 380–391.

Vershynin, R. (2012). *Introduction to the non-asymptotic analysis of random matrices*, pp. 210–268. Cambridge University Press.

Vershynin, R. (2018). *Concentration of Sums of Independent Random Variables*, pp. 11–37. Cambridge Series in Statistical and Probabilistic Mathematics. Cambridge University Press.

Walsh, D. and I. Mohr (2011). Viral subversion of the host protein synthesis machinery. *Nature Reviews Microbiology* 9(12), 860–875.

Xu, S., E. Hu, Y. Cai, Z. Xie, X. Luo, L. Zhan, W. Tang, Q. Wang, B. Liu, R. Wang, et al. (2024). Using clusterprofiler to characterize multiomics data. *Nature Protocols* 19(11), 3292–3320.

Yang, S., C. Cao, Z. Xie, and Z. Zhou (2020). Analysis of potential hub genes involved in the pathogenesis of Chinese type 1 diabetic patients. *Annals of Translational Medicine* 8, 295–295.

Zeng, T. and J. Li (2010). Maximization of negative correlations in time-course gene expression data for enhancing understanding of molecular pathways. *Nucleic Acids Research* 38(1), e1–e1.

Zhang, S., B. J. Heil, W. Mao, M. Chikina, C. S. Greene, and E. A. Heller (2024). MousiPLIER: A mouse pathway-level information extractor model. *eNeuro* 11(6).

Zhou, Y., K. Luo, L. Liang, M. Chen, and X. He (2023). A new Bayesian factor analysis method improves detection of genes and biological processes affected by perturbations in single-cell crispr screening. *Nature Methods* 20(11), 1693–1703.

Methods

Model description

Let $Y \in \mathbb{R}^{n \times p}$ be the gene expression profile, where n is the number of samples, p is the number of genes and usually $n \ll p$. Data are standardized to have mean zero and variance 1 for each column (gene). Let $y_i = (y_{i1}, \dots, y_{ip})^\top$ denote the i th row of Y for $i = 1, \dots, n$. We will denote by C the matrix of $p \times q$ gene sets, where q is the number of gene sets. Let $c_j = (c_{j1}, \dots, c_{jq})^\top \in \{0, 1\}^q$, with $c_{jl} = 1$ indicating that the gene j belongs to the gene set l for $j = 1, \dots, p$ and $l = 1, \dots, q$. To characterize the gene-gene covariance matrix while enabling dimensionality reduction informed by prior knowledge of gene sets, we let

$$y_i = \Lambda \eta_i + \epsilon_i, \quad \epsilon_i \sim N_p(0, \Sigma), \quad (1)$$

with $\eta_i = (\eta_{i1}, \dots, \eta_{ik})^\top \sim N_k(0, I_k)$ latent factors for patient i where k is the number of factors, Λ is a $p \times k$ loadings (gene weights) matrix relating these latent factors to the different gene expressions, and ϵ_i is a residual term having covariance matrix $\Sigma = \sigma^2 I_p$. Integrating out the latent factors from (1), we obtain an equivalent representation of the model as $y_i \sim N_p(0, \Lambda \Lambda^\top + \Sigma)$. In order to incorporate prior knowledge of gene sets into learning of gene expression factors, we decompose the gene weights as

$$\Lambda = C\Gamma + \Psi, \quad (2)$$

where C is the gene sets matrix, $\Gamma = \{\gamma_{lh}\}$ is a $q \times k$ sparse graphical matrix linking gene expression factors to gene sets ($\gamma_{lh} \neq 0$ if factor h is linked to gene set l), and Ψ is an unstructured $p \times k$ matrix characterizing covariance structure in the gene expressions not related to pre-existing gene sets. For identifiability reasons, we require $\Psi \in \mathcal{N}(C)$, where $\mathcal{N}(C)$ denotes the null space of C . Expressions (1)-(2) imply the following gene-gene covariance structure in the gene expression data

$$\text{cov}(y_i) = [C\Gamma + \Psi][\Gamma^\top C^\top + \Psi^\top] + \Sigma,$$

which is the sum of a low-rank and a diagonal matrix. Hence, the co-expression matrix depends on the matrix of gene sets C , which guides the inference. In particular, we have $C\Gamma = P_C\Lambda$ and $\Psi = (I - P_C)\Lambda$, where $P_C = C(C^\top C)^{-1}C^\top$ denotes the orthogonal projection matrix onto the column space of C , $\mathcal{C}(C)$. Equivalently, (2) can be represented as

$$\Lambda = B_C \Lambda_C + B_N \Lambda_N, \quad (3)$$

with $\Lambda_C \in \mathbb{R}^{q \times k}$, $\Lambda_N \in \mathbb{R}^{p-q \times k}$ and $B_C \in \mathbb{R}^{p \times q}$, $B_N \in \mathbb{R}^{p \times p-q}$ orthonormal bases onto the column space and null space of C , respectively. For a given Γ and a given basis B_C , $\Lambda_C = B_C^\top C\Gamma = B_C^\top \Lambda$. Similarly, for given B_N and Ψ , $\Lambda_N = B_N^\top \Psi = B_N^\top \Lambda$. If we let $y_{Ci} = B_C^\top y_i$ and $y_{Ni} = B_N^\top y_i$, we have

$$y_{Ci} = \Lambda_C \eta_i + \epsilon_{Ci}, \quad y_{Ni} = \Lambda_N \eta_i + \epsilon_{Ni},$$

where $\epsilon_{Ci} \sim N_q(0, \sigma^2 I_q)$, $\epsilon_{Ni} \sim N_{p-q}(0, \sigma^2 I_{p-q})$, and $y_{Ci} \perp\!\!\!\perp y_{Ni}$.

Prior Specification

Taking a Bayesian approach, we choose shrinkage priors for the elements of Λ_C and Λ_N :

$$\begin{aligned}\lambda_{Cl} \mid \sigma^2 &\sim \mathcal{N}_k(0, \tau_\Gamma^2 \sigma^2 I_k), \quad (l = 1, \dots, q), \\ \lambda_{Nl'} \mid \sigma^2 &\sim \mathcal{N}_k(0, \tau_\Psi^2 \sigma^2 I_k), \quad (l' = 1, \dots, p - q),\end{aligned}$$

with λ_{Cl} and $\lambda_{Nl'}$ denoting the l -th and l' -th rows of Λ_C and Λ_N , respectively.

This allows the data to inform about the degree to which the inferred lower-dimensional factors η_i underlying the high-dimensional y_i are linked to pre-existing gene sets. The structure also enables learning of new gene sets corresponding to genes that have non-zero loadings Λ on the same factors η_{ih} . Most importantly, we allow for different degrees of shrinkage in Λ_C and Λ_N , respectively, to accommodate cases where the strength of the signal explained by C differs from the residual one. To enhance data-adaptivity and limit the practitioner's tuning effort, we develop an empirical Bayes strategy to select the prior shrinkage coefficients τ_Γ and τ_Ψ . For instance, we show that in absence of residual signal, BASIL collapses on the simpler model $\Lambda = C\Gamma$ as $\tau_\Psi \rightarrow 0$. We complete the prior specification with an inverse-gamma prior on σ^2 , i.e. $\sigma^2 \sim IG(v_0/2, \sigma_0^2 v_0/2)$.

Posterior computation

The uncertainty in Λ_C and Λ_N is encoded in their posterior distribution

$$\begin{aligned}p(\Lambda_C, \Lambda_N \mid Y, X) &\propto \int p(Y \mid \Lambda_C, \Lambda_N, M) p(\Lambda_C) p(\Lambda_N) p(M) dM \\ &\propto \int p(\Lambda_C, \Lambda_N \mid Y, M) p(M \mid Y) dM.\end{aligned}$$

To facilitate efficient and accurate posterior approximation, we propose a pre-training approach. We start with an initial estimate of $M = [\eta_1 \ \cdots \ \eta_n]^\top$ given by $\hat{M} = \sqrt{n}U$, where $U \in \mathbb{R}^{n \times k}$ is the matrix of left singular vectors of Y associated with its k leading singular values. This is sometimes referred to as a PCA-estimate and is commonly used in the econometrics literature (Bai, 2003). Pre-training for efficient posterior approximation in factor models was proposed in Chatopadhyay et al. (2024), and further developed in Mauri and Dunson (2025a,b); Mauri et al. (2025), but none of these approaches can include prior information on gene sets. As the number of variables p increases, the marginal posterior of latent factors concentrates around a point estimate, so ignoring uncertainty in M has negligible impact on accuracy of uncertainty quantification and estimation. This approach is related to joint estimation for factor models (Chen et al., 2019, 2020; Lee et al., 2024), which is consistent in double asymptotic scenarios in which both sample size and outcome dimension diverge. We approximate the posterior distribution of Λ_C and Λ_N as follows:

$$p(\Lambda_C, \Lambda_N \mid Y) \approx p(\Lambda_C, \Lambda_N \mid Y, \hat{M}).$$

Conditionally on \hat{M} , inference on Λ_C and Λ_N corresponds to surrogate multilinear regression tasks, where \hat{M} is treated as the observed covariates matrix. Our prior specification for the elements of Λ , and σ^2 allows a conjugate update:

$$\begin{aligned}\sigma^2 | Y_C, Y_N &\sim IG\left(\frac{v_n}{2}, \frac{v_n \sigma_n^2}{2}\right), \\ \lambda_{Cl} | Y_C, \sigma^2 &\sim N_k\left(\mu_{Cl}, \frac{\sigma^2}{n + \tau_\Gamma^{-2}} I_k\right), \quad (l = 1, \dots, q), \\ \lambda_{Nl'} | Y_N, \sigma^2 &\sim N_k\left(\mu_{Nl'}, \frac{\sigma^2}{n + \tau_\Psi^{-2}} I_k\right), \quad (l' = 1, \dots, p - q),\end{aligned}$$

where

$$\begin{aligned}v_n &= v_0 + n, \\ \sigma_n^2 &= \frac{1}{v_n} \left\{ v_0 \sigma_0^2 + \sum_{l=1}^q [y_C^{(l)\top} y_C^{(l)} - (n + \tau_\Gamma^{-2}) \mu_{Cl}^\top \mu_{Cl}] + \sum_{l'=1}^{p-q} [y_N^{(l')\top} y_N^{(l')} - (n + \tau_\Psi^{-2}) \mu_{Nl'}^\top \mu_{Nl'}] \right\}, \\ \mu_{Cl} &= (\hat{M}^\top \hat{M} + \tau_\Gamma^{-2} I_k)^{-1} \hat{M}^\top y_C^{(l)} = \frac{1}{n + \tau_\Gamma^{-2}} \hat{M}^\top y_C^{(l)}, \\ \mu_{Nl'} &= (\hat{M}^\top \hat{M} + \tau_\Psi^{-2} I_k)^{-1} \hat{M}^\top y_N^{(l')} = \frac{1}{n + \tau_\Psi^{-2}} \hat{M}^\top y_N^{(l')},\end{aligned}$$

with $y_C^{(l)}$ and $y_N^{(l')}$ denoting the l -th and l' -th columns of YB_C and YB_N , respectively. Importantly, this step can be parallelized across columns of Y_C and Y_N . Moreover, because of conjugacy, we can obtain independent samples from the posterior of the loadings without the need for MCMC. As in other pre-training methods, this approach induces a posterior distribution over components of the covariance matrix that suffers from a mild undercoverage. We solve this issue by applying a simple coverage correction strategy, as in [Chattopadhyay et al. \(2024\)](#), consisting of inflating the posterior variance of Λ_C and Λ_N by the terms $\rho_C^2 > 1$ and $\rho_N^2 > 1$, respectively, which are tuned to achieve valid asymptotic frequentist coverage. The coverage corrected samples for Λ are then given by

$$\begin{aligned}\lambda_{Cl} | Y_C, \sigma^2 &\sim N_k\left(\mu_{Cl}, \frac{\sigma^2 \rho_C^2}{n + \tau_\Gamma^{-2}} I_k\right), \quad (l = 1, \dots, q) \\ \lambda_{Nl'} | Y_N, \sigma^2 &\sim N_k\left(\mu_{Nl'}, \frac{\sigma^2 \rho_N^2}{n + \tau_\Psi^{-2}} I_k\right), \quad (l' = 1, \dots, p - q).\end{aligned}$$

The posterior mean for Λ_C and Λ_N are available in closed form:

$$\begin{aligned}\mathbb{E}[\Lambda_C | -] &= [\mu_{C1} \ \dots \ \mu_{Cq}]^\top = \frac{\sqrt{n}}{n + \tau_\Gamma^{-2}} Y_C^\top U = \frac{\sqrt{n}}{n + \tau_\Gamma^{-2}} B_C^\top V D, \\ \mathbb{E}[\Lambda_N | -] &= [\mu_{N1} \ \dots \ \mu_{Np-q}]^\top = \frac{\sqrt{n}}{n + \tau_\Psi^{-2}} Y_N^\top U = \frac{\sqrt{n}}{n + \tau_\Psi^{-2}} B_N^\top V D,\end{aligned}$$

and the induced posterior means for Γ and Ψ are

$$\begin{aligned}\mathbb{E}[\Gamma | -] &= \frac{\sqrt{n}}{n + \hat{\tau}_\Gamma^{-2}} (C^\top C)^{-1} C^\top V D, \\ \mathbb{E}[\Psi | -] &= \frac{\sqrt{n}}{n + \hat{\tau}_\Psi^{-2}} (I - P_C) V D,\end{aligned}$$

where $D = \text{diag}(d_1, \dots, d_k)$, with d_l being the l -th largest singular value of Y , and $V \in \mathbb{R}^{p \times k}$ is the matrix of the associated right singular vectors of Y . It is easy to show that the induced posterior mean on the covariance matrix is given by

$$\mathbb{E}[\Lambda \Lambda^\top + \sigma^2 I_p | -] = \bar{\Lambda} \bar{\Lambda}^\top + \sigma_n^2 \frac{v_n}{v_n - 2} \left\{ 1 + \rho^2 \left(\frac{1}{n + \tau_\Gamma^{-2}} + \frac{1}{n + \tau_\Psi^{-2}} \right) \right\} I_p, \quad (4)$$

where $\bar{\Lambda} = \mathbb{E}[\Lambda | -] = C \mathbb{E}[\Gamma | -] + \mathbb{E}[\Psi | -]$. Given a sample for Λ_C and Λ_N , we obtain a sample for Λ via (3). These samples are drawn independently, substantially improving the computational efficiency over MCMC. Posterior summaries for any functional of the model parameters, including point and interval estimates, can be calculated using such samples. For instance, for given samples of Λ and σ , we can sample the latent factors of the i -th sample (the i -th row of M), via

$$\eta_i | y_i, \Lambda, \sigma^2 \sim N_k \left((\Lambda^\top \Lambda + \sigma^2 I_k)^{-1} \Lambda^\top y_i, \left(\frac{1}{\sigma^2} \Lambda^\top \Lambda + I_k \right)^{-1} \right).$$

Given N_{MC} samples of Λ and σ^2 , $\{\Lambda^{(s)}\}_{s=1}^{N_{MC}}$, $\{\sigma^{2(s)}\}_{s=1}^{N_{MC}}$, we can approximate the posterior mean for η_i via

$$\mathbb{E}[\eta_i | y_i] \approx \frac{1}{N_{MC}} \sum_{s=1}^{N_{MC}} (\Lambda^{(s)\top} \Lambda^{(s)} + \sigma^{2(s)} I_k)^{-1} \Lambda^{(s)\top} y_i.$$

To improve interpretability of the subject-specific factors, we induce sparsity in the factor matrix M by applying a varimax rotation (Kaiser, 1958). This orthogonal transformation rotates the factor axes to maximize the variance of squared factors, yielding a sparser and more interpretable factor structure.

Hyperparameter tuning

This section describes how the hyperparameters of BASIL are selected. As a criterion to select the number of factors, we use the joint likelihood based information criterion (JIC) of Chen and Li (2021),

$$\text{JIC}(k) = -2l_k + k \max(n, p) \log\{\min(n, p)\}, \quad (5)$$

where l_k is the value of the joint log-likelihood computed at the joint maximum likelihood estimate for latent factors and factor loadings when the latent dimension is equal to k . To avoid the computation of joint maximum likelihood estimates for each value of k , we approximate l_k with $l_k \approx \hat{l}_k$, where \hat{l}_k is the likelihood for the study-specific data matrix under spectral estimates, i.e. the product of the estimates for latent factors and loadings correspond to the best rank k approximation to Y . For the prior shrinkage coefficients, note that conditionally on σ^2 , the *a priori* expected values of the Frobenius norm squared of Λ_C and Λ_N are $\mathbb{E}[\|\Lambda_C\|_F^2 | \sigma^2] = \tau_\Gamma^2 \sigma^2 q k$ and $\mathbb{E}[\|\Lambda_N\|_F^2 | \sigma^2] = \tau_\Psi^2 \sigma^2 (p - q) k$. We let $L_C = \|P_C V D\|_F^2 / n$, $L_N = \|(I_p - P_C) V D\|_F^2 / n$, and $\hat{\sigma}^2 = \|(I_n - U U^\top) Y\|_2^2 / [(n - k)p]$, which are consistent estimates of $\|\Lambda_C\|_F^2$, $\|\Lambda_N\|_F^2$, and σ^2 , respectively. Thus, we set τ_Γ^2 and τ_Ψ^2 to $\hat{\tau}_\Gamma^2 = \frac{L_C}{k q \hat{\sigma}^2}$

and $\hat{\tau}_\Psi^2 = \frac{L_N}{k(p-q)\hat{\sigma}^2}$, respectively. For ρ , we take inspiration from [Chattopadhyay et al. \(2024\)](#), and for $f, g = 1, \dots, p$, we let

$$b_{fg} = \begin{cases} \left\{ 1 + \frac{\|\mu_f\|_2^2 \|\mu_g\|_2^2 + (\mu_{\mathcal{C}f}^\top \mu_g)^2}{\hat{\sigma}^2 (\|\mu_f\|_2^2 + \|\mu_g\|_2^2)} \right\}^{1/2}, & \text{if } f \neq g \\ \left(1 + \frac{\|\mu_f\|_2^2}{2\hat{\sigma}^2} \right)^{1/2}, & \text{otherwise,} \end{cases}$$

where μ_j is the j -th row of $\mathbb{E}[\Lambda | -] = C\mathbb{E}[\Gamma | -] + \mathbb{E}[\Psi | -]$. Then, we set $\rho = \binom{q}{2}^{-1} \sum_{1 \leq f \leq g \leq p} b_{fg}$, which allows control of the coverage on average across entries. Finally, we set $v_0 = 1$ and $\sigma_0^2 = 1$.

Theoretical guarantees

We start by introducing notation. For a matrix A , we denote by $\|A\|$, $\|A\|_2$ its spectral and Frobenius norm, respectively, by $s_l(A)$ its l -th largest singular value, and by $tr(A)$ its trace. Moreover, for two sequences $(a_n)_{n \leq 1}$, $(b_n)_{n \leq 1}$, we say $a_n \lesssim b_n$ if there exist two constants $N_0 < \infty$ and $C < \infty$, such that $a_n \leq Cb_n$ for every $n > N_0$. We say $a_n \asymp b_n$ if and only if $a_n \lesssim b_n$ and $b_n \lesssim a_n$.

We enumerate a few regularity conditions.

Assumption 1. Data are generated under model (1), with true loading matrix $\Lambda_0 = C\Gamma_0 + \Psi_0$, and error variance σ_0^2 . Moreover, we have $C\Gamma_0 \perp \Psi_0$. We denote by M_0 the true latent factors.

The condition $C\Gamma_0 \perp \Psi_0$ in Assumption 1 is needed to ensure the identifiability of the parameters Γ and Ψ . Indeed if such a condition was not imposed, for some given values of the parameters, Γ and Ψ , one could let $\tilde{\Gamma} = 0$ and $\tilde{\Psi} = \Psi + C\Gamma$. It is easy to verify that (Γ, Ψ) and $(\tilde{\Gamma}, \tilde{\Psi})$ induce the same distribution for y . Imposing this condition resolves this non-identifiability due to the uniqueness of the decomposition of vectors as a sum of elements lying in orthogonal subspaces.

Assumption 2. We let $p = p_n \rightarrow \infty$ and $\log(p_n)/n = \mathcal{O}(1)$ as $n \rightarrow \infty$.

Assumption 2 requires the dimensionality to grow with the sample size no faster than a polynomial rate. Considering a growing dimension is reasonable since in genomics we typically have $p \gg n$.

Assumption 3. We have $s_l(\Lambda) \asymp \sqrt{p}$, which implies that either $s_l(C\Gamma_0) \asymp \sqrt{p}$ or $s_l(\Psi_0) \asymp \sqrt{p}$, for $l = 1, \dots, k$.

Assumption 3 allows the systematic component of the variation to be distinguished from pure noise.

Assumption 4. The number of latent factors k is known.

While this Assumption may not hold in practice, the JIC defined in (5) has been shown to provide consistent estimates for k under mild assumptions ([Chen and Li, 2021](#)).

First, we propose the following point estimator for the idiosyncratic variance, $\hat{\sigma}^2 = \|(I_n - UU^\top)Y\|_2^2 / [(n - k)p]$, and show its consistency. All the proofs are given in the Supplementary.

Proposition 1. *Under Assumptions 1–4, as $n \rightarrow \infty$, with probability at least $1 - o(1)$, we have*

$$\hat{\sigma}^2 = \sigma_0^2 + r_n,$$

where $|r_n| \lesssim \frac{1}{\sqrt{n}} + \frac{1}{\sqrt{p_n}}$.

Next, we characterize the behaviour of the prior shrinkage parameters in two special cases, that is when all the variation is explained by either known or new pathways.

Proposition 2. *Under Assumptions 1 to 4, as $n \rightarrow \infty$, if $\Psi_0 = 0$, or, equivalently, there are no new pathways active, $\hat{\tau}_\Psi \rightarrow 0$ in probability, and, if $\Gamma_0 = 0$, or, equivalently, there are no known pathways active, $\hat{\tau}_\Gamma \rightarrow 0$ in probability.*

The proposition 2 characterizes the behavior of BASIL in two specific scenarios. When there are no new pathways active and all the systematic variability is explained by known pathways, or, formally, $\Psi = 0$, the prior variance parameter controlling the shrinkage of Ψ converges to 0, and BASIL collapses on the simpler model $\Lambda = C\Gamma$. Analogously, when all variability is explained by new pathways, $\Gamma = 0$, the prior variance parameter controlling the shrinkage of Γ converges to 0, and BASIL collapses on the simpler model $\Lambda = \Psi$. Therefore, our procedure adaptively selects the amount of shrinkage to apply to structured and unstructured variability and chooses simpler model specifications when adequate.

Additional details about the simulation experiments

We conducted a simulation study to assess the performance of BASIL in computing time and the accuracy of estimation and quantification of uncertainty for the correlation matrix between genes. We simulate data under the BASIL model (1)-(2) with sample size $n = 500$, number of genes $p \in \{1000, 3000\}$ and set $\sigma^2 = 15$ and $k = 10$. We considered two different scenarios: one in which there is strong gene ontology information ($\tau_\Gamma^2 = 0.7$, $\tau_\Psi^2 = 0.1$) and one in which there is low gene ontology information and more unstructured variability ($\tau_\Gamma^2 = 0.4$, $\tau_\Psi^2 = 0.7$). We obtain the matrix of gene sets C using the `msigdbr` R package that provides access to gene sets from the Molecular Signatures Database. Specifically, we used the molecular function subcategory of the gene ontology category. For each configuration, we replicate the experiments 25 times. We evaluate estimation accuracy in reconstructing $\Lambda_0\Lambda_0^\top$ via the Frobenius norm of the difference of the estimate and true parameter scaled by $\|\Lambda_0\Lambda_0^\top\|$.

We compare with PLIER (Mao et al., 2019) and ROTATE (Ročková and George, 2016), a computationally efficient factor model based on an expectation-maximization (EM) algorithm that cannot incorporate information on gene ontology. For PLIER, we used the default settings for hyperparameter selection and estimated the low rank component of the gene covariance matrix with $(\hat{\Lambda}(\hat{M}^\top \hat{M})\hat{\Lambda}^\top)/n$, where $\hat{\Lambda}$ and \hat{M} are estimates for loadings and latent factors, respectively. Since

ROTATE does not provide a default mechanism for selecting the number of factors, we set it to the true number, thereby giving this method an advantage. The performance of ROTATE tended to degrade when the number of factors was set at a value greater than k in our preliminary experiments.

To assess BASIL’s performance in uncertainty quantification, we evaluate the frequentist coverage of the posterior credible intervals for $\Lambda\Lambda^\top$. Specifically, we consider the frequentist coverage of 95% credible intervals on average across the entries of a 200×200 submatrix of $\Lambda\Lambda^\top$.

Out-of-sample predictive performance for RNA-seq data

We tested the out-of-sample predictive performance of competing methods in the two datasets analyzed (whole-blood RNA seq data and global fever data). For each data set, we perform 50 random 80%–20% train-test splits. We fit each method in the training set and compute the log-likelihood in the test set \mathcal{Y}_{test} , which, for a given estimator of the covariance $\hat{\Sigma}$, is given by

$$l(\hat{\Sigma}) = -\frac{n_{test}}{2} \log (2\pi|\hat{\Sigma}|) - \frac{1}{2} \sum_{y \in \mathcal{Y}_{test}} y^\top \hat{\Sigma}^{-1} y,$$

where n_{test} denotes the size of the test set. For BASIL, we used the posterior mean to estimate the covariance. For PLIER, we use the same adjustment described in the simulation section for the low-rank component and let $\hat{\Sigma} = \hat{\Lambda}(\hat{M}^\top \hat{M})/n\hat{\Lambda}^\top + \hat{\sigma}^2 I_p$, where $\hat{\sigma}^2$ is the empirical variance of the residual variability in the training set. We set the maximum number of latent factors for the criterion in (5) and ROTATE to the minimum number of principal components of the training data explaining at least 80% of the variability. Both BASIL and PLIER are fitted using the latent dimension estimated via the criterion in (5). Fig. 6 shows the out-of-sample log-likelihood across the 50 random splits.

In terms of predictive accuracy, the three methodologies perform comparably on the whole blood data set of [Mao et al. \(2019\)](#), while, on the global fever data set of [Ko et al. \(2023\)](#), ROTATE is the worst performing method, and BASIL slightly outperforms PLIER. Although the primary goal of BASIL is interpretable dimensionality reduction rather than prediction, out-of-sample predictive performance provides a critical assessment of model adequacy. Strong predictive performance indicates that the learned underlying representation captures the biological signal in the gene co-expression patterns, rather than overfitting to training data. The comparable or improved performance of BASIL thus validates that our modeling framework is sufficiently flexible to accurately characterize the underlying structure of gene co-regulation.

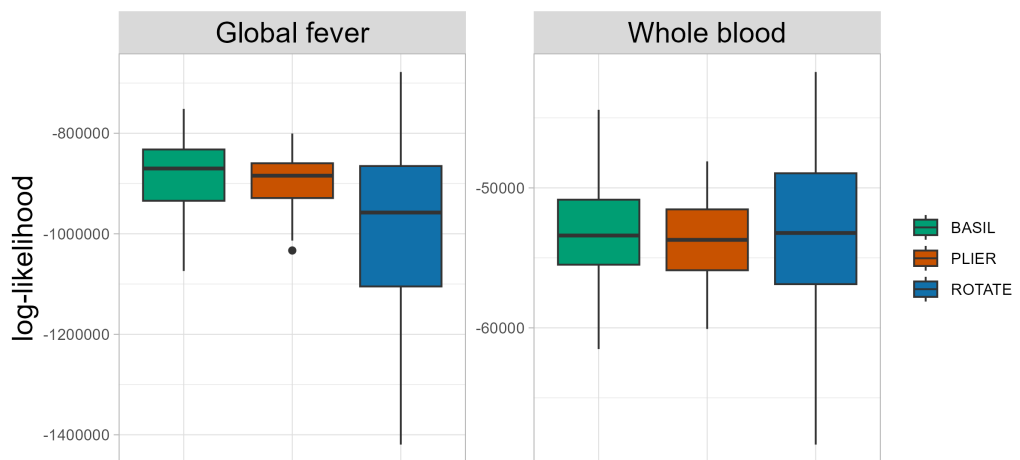


Figure 6: **Out-of-sample log-likelihood.** Out-of-sample log-likelihood of BASIL (green), PLIER (red), and ROTATE (blue) across 50 random 80% – 20% train-test splits.

Supplementary Material for “Pathway-based Bayesian factor models for gene expression data”

Proofs of theoretical results

Proof of the main result

Proof of Proposition 1. First, consider the following decomposition

$$(I_n - UU^\top)Y = (I_n - U_0U_0^\top)Y + (U_0U_0^\top - UU^\top)Y = (I_n - U_0U_0^\top)E + (U_0U_0^\top - UU^\top)Y.$$

Thus,

$$\|(I_n - UU^\top)Y\|_2^2 = \|(I_n - U_0U_0^\top)E\|_2^2 + \|(U_0U_0^\top - UU^\top)Y\|_2^2 + 2\text{tr}(E^\top(I_n - U_0U_0^\top)(U_0U_0^\top - UU^\top)Y).$$

Next, we analyze each term separately.

1. $\|(I_n - U_0U_0^\top)E\|_2^2 \sim \sigma_0 \chi_{(n-k)p}^2$, where χ_ν^2 denotes the χ -squared distribution with ν degrees of freedom.
2. With probability at least $1 - o(1)$, $\|(U_0U_0^\top - UU^\top)Y\|_2 \lesssim \|U_0U_0^\top - UU^\top\| \|Y\|_2 \lesssim \frac{\sqrt{p}}{\sqrt{n}} + \frac{\sqrt{n}}{\sqrt{p}}$, since, with probability at least $1 - o(1)$, $\|UU^\top - U_0U_0^\top\| \lesssim \frac{1}{n} + \frac{1}{p}$ by Proposition 3 and $\|Y\|_2 \lesssim \sqrt{np}$ by Proposition 5.
3. With probability at least $1 - o(1)$, $|\text{tr}(E^\top(I_n - U_0U_0^\top)(U_0U_0^\top - UU^\top)Y)| \leq \|E\|_2 \|(U_0U_0^\top - UU^\top)Y\|_2 \lesssim \sqrt{n} + \sqrt{p} + \frac{p}{\sqrt{n}} + \frac{n}{\sqrt{p}}$, since, with probability at least $1 - o(1)$, $\|(U_0U_0^\top - UU^\top)Y\|_2 \lesssim \frac{\sqrt{p}}{\sqrt{n}} + \frac{\sqrt{n}}{\sqrt{p}}$ by the previous point and $\|E\|_2 \lesssim \sqrt{np}$ by Proposition 4.

Moreover, we have $\left| \frac{\|(I_n - U_0U_0^\top)E\|_2^2}{(n-k)p} - \sigma_0^2 \right| \lesssim \frac{1}{\sqrt{n}} + \frac{1}{\sqrt{p}}$, with probability at least $1 - o(1)$, by Corollary 2.8.3 of Vershynin (2018). Combining all of the above and letting $r_n = \hat{\sigma}^2 - \sigma_0^2$, we have

$$|r_n| \lesssim \frac{1}{\sqrt{n}} + \frac{1}{\sqrt{p}} + \frac{1}{(n-k)p} \left(\frac{p}{n} + \frac{n}{p} + \sqrt{n} + \sqrt{p} + \frac{p}{\sqrt{n}} + \frac{n}{\sqrt{p}} \right) \lesssim \frac{1}{\sqrt{n}} + \frac{1}{\sqrt{p}},$$

with probability at least $1 - o(1)$. □

Proof of Proposition 2. It follows as a corollary from Propositions 1 and 6. □

Auxiliary Results

Proposition 3 (Proposition 3.5 of Chattopadhyay et al. (2024)). *Let U be the matrix of left singular vectors associated to the leading k singular values of Y and U_0 be the matrix of left singular vectors of $M_0\Lambda_0^\top$. Then, under Assumptions 1–4, as $n \rightarrow \infty$, with probability at least $1 - o(1)$, we have*

$$\|UU^\top - U_0U_0^\top\| \lesssim \frac{1}{n} + \frac{1}{p}.$$

Proposition 4. Under Assumption 1–3, we have

$$\begin{aligned} \|EP_C\| &\lesssim \sqrt{n} + \sqrt{q}, & \|E(I_p - P_C)\| &\lesssim \sqrt{n} + \sqrt{p - q}, \\ \|EP_C\|_2 &\lesssim \sqrt{nq}, & \|E(I_p - P_C)\|_2 &\lesssim \sqrt{n(p - q)}, \\ \|U_0^\top EP_C\|_2 &\lesssim \sqrt{kq}, & \|U_0^\top E(I_p - P_C)\|_2 &\lesssim \sqrt{k(p - q)}, \end{aligned}$$

with probability at least $1 - o(1)$.

Proof of Proposition 5. The results follow from Corollary 5.35 of Vershynin (2012) after noting that $\|EP_C\|_2 = \|EB_C\|_2$, $\|E(I_p - P_C)\|_2 = \|EB_N\|_2$, $\|U_0^\top EP_C\|_2 = \|U_0^\top EB_C\|_2$, and $\|U_0^\top E(I_p - P_C)\|_2 = \|U_0^\top EB_N\|_2$, with $EB_C \in \mathbb{R}^{n \times q}$, $EB_N \in \mathbb{R}^{n \times (p-q)}$, $U_0^\top EB_C \in \mathbb{R}^{k \times q}$, and $U_0^\top EB_N \in \mathbb{R}^{k \times (p-q)}$ having entries being distributed as independent Gaussian random variables with 0 mean and σ_0 standard deviation. \square

Proposition 5. Under Assumption 1–3, we have

$$\|YP_C\|_2 \lesssim \sqrt{n}\|C\Gamma_0\|_2 + \sqrt{nq}, \quad \|Y(I - P_C)\|_2 \lesssim \sqrt{n}\|\Psi_0\|_2 + \sqrt{n(p - q)},$$

with probability $1 - o(1)$.

Proof of Proposition 5. First, note $YP_C = M_0\Gamma_0^\top C^\top + EP_C$. Next, note that, with probability at least $1 - o(1)$, $\|M_0\Gamma_0^\top C^\top\|_2 \leq \|M_0\|\|\Gamma_0^\top C^\top\|_2 \lesssim (\sqrt{n} + \sqrt{k})\|\Gamma_0^\top C^\top\|_2 \asymp \sqrt{n}\|\Gamma_0^\top C^\top\|_2$, since $\|M_0\| \lesssim \sqrt{n} + \sqrt{k}$, with probability at least $1 - o(1)$, by Corollary 5.35 of Vershynin (2012), proving the first result in combination with Proposition 4. The second result is proven with analogous steps. \square

Then, consider the two following quantities, $L_C = \|P_C VD\|_F^2/n$, $L_N = \|(I_p - P_C)V D\|_F^2/n$, measuring the magnitude of the signal explained by known and unknown pathways respectively.

Proposition 6. Under Assumptions 1–4, as $n \rightarrow \infty$, we have

$$L_C = \|C\Gamma_0\|_2^2 + r_{C,n}, \quad L_N = \|\Psi_0\|_2^2 + r_{N,n},$$

where $|r_{C,n}| \lesssim \|C\Gamma_0\|_2^2(1/\sqrt{n} + 1/p) + \|C\Gamma_0\|_2(1 + \sqrt{q/n}) + q/n + q/p$ and $|r_{N,n}| \lesssim \|\Psi_0\|_2^2(1/\sqrt{n} + 1/p) + \|\Psi_0\|_2(1 + \sqrt{(p-q)/n}) + (p-q)/n + (p-q)/p$, with probability at least $1 - o(1)$.

Proof of Proposition 6. We only show the result for L_C , since the one for L_N follows with similar steps. Since $P_C VD = P_C Y^\top U$, we have the following decomposition,

$$\begin{aligned} P_C VD^2 V^\top P_C &= P_C Y^\top U U^\top Y P_C = P_C Y^\top U_0 U_0^\top Y P_C + P_C Y^\top (U U^\top - U_0 U_0^\top) Y P_C \\ &= C\Gamma_0 M_0^\top M_0 \Gamma_0^\top C^\top + C\Gamma_0 M_0^\top EP_C + P_C E^\top M_0 \Gamma_0^\top C^\top + P_C E^\top U_0 U_0^\top EP_C \\ &\quad + P_C Y^\top (U U^\top - U_0 U_0^\top) Y P_C \\ &= n C\Gamma_0 \Gamma_0^\top C^\top + C\Gamma_0 (M_0^\top M_0 - n I_k) \Gamma_0^\top C^\top + C\Gamma_0 M_0^\top EP_C + P_C E^\top M_0 \Gamma_0^\top C^\top \\ &\quad + P_C E^\top U_0 U_0^\top EP_C + P_C Y^\top (U U^\top - U_0 U_0^\top) Y P_C \end{aligned}$$

Next, we bound each term.

1. With probability at least $1 - o(1)$, we have $\|C\Gamma_0(M_0^\top M_0 - nI_k)\Gamma_0^\top C^\top\|_2 \leq \|C\Gamma_0\|_2^2 \|M_0^\top M_0 - nI_k\| \lesssim \|C\Gamma_0\|_2^2 (\sqrt{n} + \sqrt{k})$, since $\|M_0^\top M_0 - nI_k\| \lesssim \sqrt{n} + \sqrt{k}$ by Corollary 5.35 of [Vershynin \(2012\)](#).

2. With probability at least $1 - o(1)$, we have

$$\|C\Gamma_0 M_0^\top EP_C\|_2 \leq \|C\Gamma_0\|_2 \|M_0\| \|EP_C\| \lesssim \|C\Gamma_0\|_2 (\sqrt{n} + \sqrt{k}) (\sqrt{n} + \sqrt{q}) \lesssim \|C\Gamma_0\|_2 (n + \sqrt{nq}).$$

since, with probability at least $1 - o(1)$, $\|EP_C\| \lesssim \sqrt{n} + \sqrt{q}$ by Proposition 4, and $\|M_0\| \lesssim \sqrt{n} + \sqrt{k}$ by Corollary 5.35 of [Vershynin \(2012\)](#)

3. With probability at least $1 - o(1)$, we have

$$\|P_C E^\top U_0 U_0^\top EP_C\|_2 \leq \|P_C E^\top U_0\|_2^2 \lesssim \sqrt{kq}$$

by Proposition 4.

4. With probability at least $1 - o(1)$, we have

$$\begin{aligned} \|P_C Y^\top (UU^\top - U_0 U_0^\top) Y P_C\|_2 &\leq \|Y P_C\|_2^2 \|UU^\top - U_0 U_0^\top\| \lesssim (\sqrt{n} \|C\Gamma\|_2 + \sqrt{nq})^2 \left(\frac{1}{n} + \frac{1}{p}\right) \\ &= (\|C\Gamma\|_2^2 + q) \left(1 + \frac{n}{p}\right) \end{aligned}$$

since, with probability at least $1 - o(1)$, $\|UU^\top - U_0 U_0^\top\| \lesssim \frac{1}{n} + \frac{1}{p}$ by Proposition 3 and $\|Y P_C\|_2 \lesssim \sqrt{n} \|C\Gamma\| + \sqrt{nq}$ by Proposition 5.

Combining all the above and letting $r_{\mathcal{C},n} = L_{\mathcal{C}} - \|C\Gamma_0\|_2^2$, we obtain

$$|r_{\mathcal{C},n}| \lesssim \|C\Gamma_0\|_2^2 \left(\frac{1}{\sqrt{n}} + \frac{1}{p}\right) + \|C\Gamma_0\|_2 \left(1 + \sqrt{\frac{q}{n}}\right) + \frac{q}{n} + \frac{q}{p}$$

with probability at least $1 - o(1)$. Analogous steps lead to $|r_{\mathcal{N},n}| \lesssim \|\Psi_0\|_2^2 (1/\sqrt{n} + 1/p) + \|\Psi_0\|_2 (1 + \sqrt{(p-q)/n}) + (p-q)/n + (p-q)/p$, with $r_{\mathcal{N},n} = L_{\mathcal{N}} - \|\Psi_0\|_2^2$. \square

Details on global fever data

The global fever cohort included 102 participants with bacterial infections (42 bloodstream infections and 60 bacterial zoonoses), 125 with viral infections (82 respiratory and 43 dengue), and 67 with non-infectious illnesses (e.g., pulmonary embolism, congestive heart failure, COPD/asthma, cancer, and autoimmune disorders) ([Ko et al., 2023](#)). Pathogens stratified by country are reported in Table 1.

To construct a gene set matrix, we first mapped RefSeq transcript identifiers from the GSE211567 normalized expression data to Ensembl gene identifiers using the org.Hs.eg.db annotation database. We retrieved Gene Ontology Molecular Function (GO:MF) gene sets from the Molecular Signatures Database (MSigDB) for Homo sapiens (collection C5) and merged these annotations with our identifier

Table 1: Pathogen stratified by country in the global fever dataset.

Pathogen	Infection type	Sri Lanka	United States
Coxiella burnetii	Bacterial	3	0
Dengue	Viral	43	0
Enterobacter	Bacterial	0	17
Influenza A and B	Viral	38	29
Leptospira	Bacterial	30	0
Non-infection	Non-infection	0	67
Respiratory virus, other	Viral	0	13
Rickettsia	Bacterial	27	0
Staphylococcus	Bacterial	0	10
Streptococcus	Bacterial	0	14

mappings. We then generated a binary gene sets matrix where rows represent genes and columns represent gene sets, with entries indicating gene membership (1) or non-membership (0) in each set. To ensure robust downstream analysis, we filtered out pathways with fewer than 10 genes and genes that were not annotated to any gene set.

Gene set enrichment analysis for global fever data

The BASIL factors were interpreted by applying gene set enrichment analysis (GSEA) to the loadings separately for each factor. While the Gene Ontology Molecular Function collection was used to construct the factors to reduce selection bias in gene set curation, generating contextualized interpretations using this collection is challenging. Therefore, the human Reactome pathways ([Ligtenberg, 2025](#)) were used in the GSEA. The Ensemble identifiers were mapped to their Entrez counterparts using AnnotationDbi ([Pagès et al., 2025](#)), and Entrez identifiers with multiple loadings were summarized using the median. GSEA was carried out using fast GSEA ([Korotkevich et al., 2016](#)) within the clusterProfiler package ([Xu et al., 2024](#)). The Reactome pathways with 10-1,000 Entrez identifiers were used, and 100,000 permutations of the FGSEA-simple procedure were run to estimate p-values for those pathways. Pathways with a false discovery rate $\leq 5\%$ were used to construct network diagrams that could help to identify summary interpretations for each factor ([Csárdi et al., 2026](#)). Pathways with a Jaccard index exceeding 0.4 were grouped, and then singleton and doublet groups were removed. Lastly, community detection was applied to generate homogenous groups for interpretation. Figure 7 shows the pairwise plots for the elements of the first ten factors, colored by different pathogens.

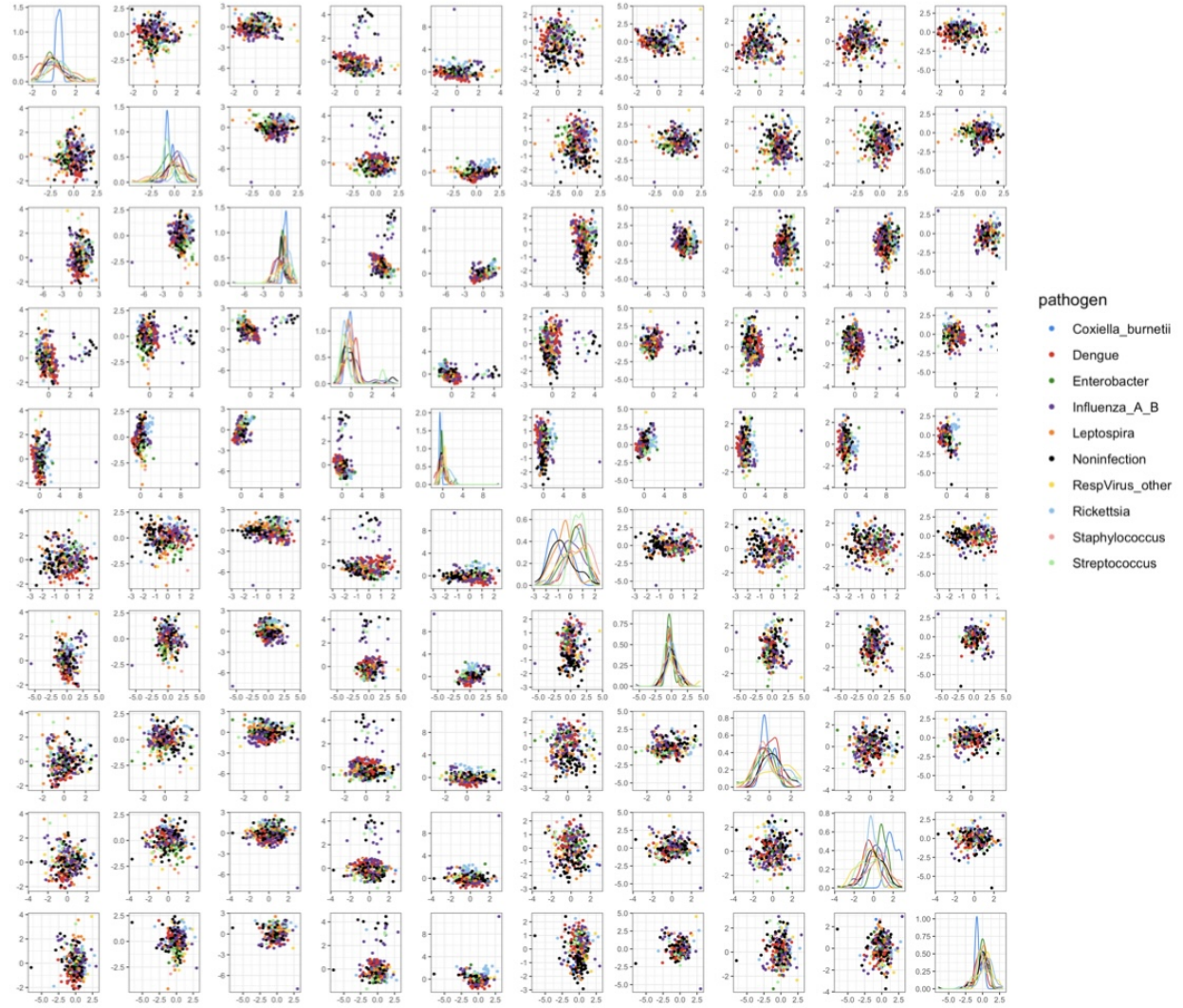


Figure 7: **Pairwise plots of latent variable values.** Pairwise plots for the elements of M are shown for the first ten factors. The sample-level points are colored by the pathogen.